BELLCOMM, INC.
955 L'ENFANT PLAZA NORTH, S.W. WASHINGTON, D. C. 20024

B70 09026

SUBJECT: Preliminary S-IVB POGO Stability Analysis - Case 320

DATE: September 11, 1970

FROM: J. J. O'Connor

ABSTRACT

The one engine configuration of the S-IVB stage leads to a simple POGO stability model which was further simplified by excluding the fuel suction line and the fuel side of the J-2 engine. The Rocketdyne engine transfer function for an NPSH of 50' and a mixture ratio of 5.0 was used. A LOX line frequency of 24 Hz was selected as a compromise between the Rocketdyne data of 25.3 Hz and the indications of 22.5 to 24 Hz found in the inflight spectrograms. The Boeing structures data of August 1, 1970, was used with a modified tank pressure coefficient.

The zero-phase gains for the eight time points were calculated by opening the loop at total force on the engine gimbal. There is a 16 Hz mode with only 2 dB of margin at burnout and this seems to agree with the inflight spectrograms. There is a 19 Hz mode during the first burn, but its 20 to 30 dB margin would not predict its clear appearance on the spectrograms. Perhaps this will be modified by Boeing's next structures update, due mid-September, which will include an elastic body analysis of the engine thrust structure.

BELLCOMM, INC.
955 L'ENFANT PLAZA NORTH, S.W. WASHINGTON, D.C. 20024

B70 09026

SUBJECT: Preliminary S-IVB POGO Stability Analysis - Case 320

DATE: September 11, 1970

FROM: J. J. O'Connor

MEMORANDUM FOR FILE

INTRODUCTION

The results of our preliminary analysis of S-IVB POGO stability were presented at the MSFC POGO Working Group Meeting of August 26-27, 1970. This memorandum, to be distributed to the attendees listed in Table I, will briefly describe the presentation.

BASIC STABILITY MODEL

The S-IVB POGO stability model is simplified by the fact that the S-IVB stage has only one engine while the S-IC and S-II stages each have five engines. Based on our S-II POGO experience we have further simplified the model by not including the fuel suction line and the fuel side of the J-2 engine.

The resulting model, shown on Figure 1, consists of Structure, LOX Line and Engine. The Aos block represents the oxidizer suction line area feedback. Since the structures model does not include the mass of the propellant in the suction lines, this Aos can be considered as a modification of the structure, as shown in Figure 1a. From a stability point of view, however, it is just as valid to consider Aos as a modification of the engine transfer function, as shown in Figure 1b. It is the configuration of Figure 1b which leads us to open the loop for stability analysis at the total force F; this is the total force acting on the engine gimbal block.

STRUCTURES BLOCK

The detalied POGO stability model, Figure 2, uses n structural modes where n is adjustable depending on the available data and the type of analysis desired. The numerical values for the structure were obtained from the Boeing Memorandum 5-9430-H-177 dated August 1, 1970. The Boeing report gave the pressure coefficient c_i which we converted as shown on Figure 2.

ENGINE BLOCK

The engine transfer function depends on Net Positive Suction Head, NPSH, and Engine Mixture Ratio, EMR. Examination of S-IVB flight data led us to specify an NPSH of 50' and an EMR of 5.0. The appropriate Rocketdyne transfer function was selected and the frequency response of the engine is shown in Figure 3. This figure also shows the Aos modification of the engine gain; it reduces the gain by 2 dB at low frequencies, increases it by 3 dB at high frequencies and adds about 10 degrees of phase lag at high frequencies.

LOX LINE BLOCK

The lumped-parameter line model shown in Figure 2 contains only one mode, the first resonance. The analysis actually used three modes which were derived from a continuous model of the line.

The line termination impedance has been separated on Figure 2 into the bubble cavitation compliance C_{bo} and the pump inlet admittance $\frac{\partial \dot{W}}{\partial P}_{os}$. This latter term is the residual of the Rocketdyne dual-compliance line termination impedance; we separate out C_{bo} in order to adjust the line frequency. Observations of our spectrograms indicate inflight line frequencies in the 22.5 to 24 Hz range while the Rocketdyne compliance would lead to a line frequency of 25.3 Hz. We selected a 24 Hz line because it is within the range of flight data and does least violence to the Rocketdyne data.

The line response is shown in Figure 4. The combined response of the line and the modified engine is also shown in Figure 4. Reference to Figure 1 shows that the combined response relates (one) output of the structures block, $\ddot{X}_G$, to input of the structures block, F. Therefore, this combined response could be considered as a POGO selectivity function in the selection of the more important longitudinal modes of the structure. That is, a mode with a given gain at 24 Hz would contribute 20 dB more to the open-loop response than a mode at 4 Hz with the same gain.

SELECTION OF STRUCTURAL MODES

The Boeing Memorandum contained structural data for four time points during the S-IVB first burn and four time points for the second burn. We decided that there were too few time points to interpolate the data, so our stability

analysis would be limited to the eight time points for which we have data.

The Boeing coupled model produces pitch, yaw and torsonial modes as well as the desired longitudinal modes, and the data consisted of 49 modes for each of the eight time points. Further, Figure 2 shows two outputs for the structures block. One is tank bottom pressure, P_T, which is applied directly to the top of the suction line. The other is engine gimbal acceleration, $\ddot{X}_G$, which converts into relative weight flow, $\dot{W}_p$, due to pump motion, and it is applied to the bottom of the line. We must find a method of scaling the two outputs of the structures block in order to select the more significant modes. Figure 5 shows the exact equation of a continuous model of the suction line, and in general, the scaling between the two inputs does depend on frequency, ω. However, under the assumption of an acoustically short line, the gimbal acceleration $\ddot{X}_G$ can be scaled by $\rho\ell/g$ to an equivalent pressure at the top of the line. For the S-IVB this scale factor is $3.08 \frac{\text{psi}}{\text{in/sec}^2}$

The peak resonant transmission for the $i^{\underline{th}}$ mode, g_i in psi/lbf, is defined as

$$g_i = \tilde{P}_{T_i} + (3.08)\ \tilde{\ddot{X}}_{G_i} = \left| \frac{c_i}{\omega_i^2} \frac{\phi_{gi}}{2\zeta_i M_i} \right| + (3.08) \left| \phi_{gi} \frac{\phi_{gi}}{2\zeta_i M_i} \right|$$

where the pressure coefficient c_i, the normalized deflection at the gimbal ϕ_{gi}, the mode frequency ω_i, the damping ζ_i and the equivalent mass M_i are obtained from the Boeing Memorandum. The values of g_i, expressed in dB, for the 25 higher gain modes of the 49 mode total are listed in Table II; the rank, mode number and the mode frequency are also listed.

In our initial handling of the data we informally obtained a scan of the data which ranked the "top" 15 modes. We selected the "top" 9 of these 15 for our first stability run. These modes are identified on Table II where it is seen that the "top" 9 or the "top" 15 do not always occupy the top ranks. This is due, in part, to the scaling used in the scan to calculate g ; it appears that the scan overemphasized the first term, $\tilde{P}_T$, at the expense of the second one, $\tilde{\ddot{X}}_G$. The mixed ranks are also due, in part, to the fact that the POGO selectivity frequency function was not applied to the data of Table II.

It should be noted that the scaling of g_i and the application of the POGO selectivity function affect only the choice of modes to be used in the stability analysis; they do not affect the resulting stability margins. Of course, there is always the possibility that a poor selection will overlook the least stable mode. This was not the case with the nine mode scan as confirmed by a later stability analysis using all 49 modes, as discussed in the next section.

STABILITY RESULTS

Using the nine modes identified on Table II and the line and engine responses of Figures 3 and 4, we derived the stability margins for the eight time points. That is, we calculated the zero phase gains, which are the crossings of the positive real axis of the Nyquist plots, when the loop is opened at total force, as shown in Figure 2. The zero phase gains, expressed in dB, are plotted against flight time in Figure 6; the data are labeled to show the frequency for each stability point.

The pressure coefficient c_i of the Boeing report should be used in a displacement type of equation; we convert it to h'_{ti}, as shown on Figure 2, and use in an acceleration type of equation. The difference between these two approaches can be seen on Figure 7. While the characteristics at the peak response are the same either way, there are questions about the off-resonance response and the contributions of other modes. To determine if this affected the calculated margins, we made a stability run without any pressure contribution, i.e., we disconnected the LOX tank from the line. Both sets of margins are listed in Table III. The table gives the data to three figures only to show how little difference there is with a complete absence of the pressure term. The difference of hundredths of a Hz and tenths of a dB could be due to the accuracy of interpolating the data.

Another run with all 49 modes including the pressure term was made, and the resulting margins are also listed in Table III. Again the differences are so slight as to be meaningless.

Table III shows one or two of the possible three margins are missing at some entries. The margins are in the 30 to 50 dB range and study of the Nyquist plots shows that small changes in these minor lobes cause them to miss the positive real axis. In fact, the Nyquist plots are more affected by the pressure term than Table III would indicate.

This is because the larger lobes which control the margins listed on Table III are due to gimbal response, not to tank pressure.

DISCUSSION

Having established that the stability plot of Figure 6 is not sensitive to our handling of tank pressure nor to the particular nine modes used in the analysis, a few comments on the S-IVB POGO stability are in order.

The 9 to 16 Hz mode which starts with 40 dB margin and ends with 2 dB margin is probably a valid result and is agreement with the flight spectrograms. This mode had been observed in previous S-IVB POGO stability analyses.

The 19 Hz mode during the first burn is a new result of the structures model and agrees with the frequency seen in the flight spectrograms. The calculated margins of 20 to 30 dB seem too large for a signal which is so manifest on the spectrograms. Perhaps this questionable result is due to the rigid thrust structure which had to be assumed in this update of the structure. The next update, due mid-September, will involve a flexible thrust structure and this may change the margin of the 19 Hz mode.

It can be said that the incorporation of a hydroelastic model for the LOX tank has not generated significant tank pressure terms but has affected the structural gains seen at the engine gimbal.

It would seem that the stability margins of Figure 6 are not critically dependent on line or engine transfer functions. For one thing the stability margins at 16 to 19 Hz are below any major gain amplification of the line. For another thing the margins are not "phase stabilized," that is, the crossings on the Nyquist plot are near the maximum of the lobes.

J. J. O'Connor

2031-JJO-ajj

Attachments

TABLE I

ATTENDANCE LIST

POGO WORKING GROUP MEETING

26-27 AUGUST 1970

J. Farrow	MSFC/S&E-ASTN-AD
T. Bullock	MSFC/S&E-ASTN-ADL
R. D. Vaage	Martin Marietta
R. J. Farrell	Martin Marietta
A. Rasumoff	TRW Systems
R. Winje	TRW Systems
J. Fenwick	Rocketdyne
J. J. O'Connor	Bellcomm
D. C. Wade	NASA/MSC
W. F. LaHatte	MSFC/PM-SAT-S-II
G. F. Riley	Boeing-Huntsville
L. E. Kraft	NR/SD
H. R. Wiener	NR/SD
R. Schwartz	NR/SD
J. Sterett	MSFC/S&E-ASTN-A
M. E. Campbell	NR/SD
M. A. Mezzacappa	NR/SD
D. DiMaggio	NR/SD
L. McTigue	Boeing-Huntsville
S. Petrilla	NR/SD
D. R. Gosdin	MSFC/S&E-ASTN-EPS
M. J. Morgan	MDAC
L. M. Olsen	MDAC
E. H. Hughes	Boeing/WDC
J. I. Kistle	NASA/Washington (MAT)
J. S. Andrews	Boeing/Houston
W. R. Marlowe	NASA/MSC/PM-MO-F
W. L. Ray	MSFC/S&E-ASTN-TSJ
O. R. Goetz	MSFC/S&E-ASTN-T
R. G. Zagrodzky	MSFC/S&E-ASTN-XSH
W. A. Jarinen	NORTHROP/Huntsville
H. P. Stinson	MSFC/S&E-ASTN-PPA
F. S. Wojtalik	MSFC/S&E-ASTR-S
J. J. Nichols	MSFC/S&E-ASTN-ADS
R. C. Spink	MSFC/S&E-ASTN-PFB
A. L. Worlund	MSFC/S&E-ASTN-PF
R. M. Hunt	MSFC/S&E-ASTN-A
R. L. Grimm	Rocketdyne
J. E. Harbison	MSFC/S&E-ASTN-ADL
En N. Jackson	NR/SD - Huntsville
R. P. Rice	MSFC/PM-SAT-S-IVB
V. L. Glasgow	Boeing-Huntsville
Larry Kiefling	MSFC/S&E-AERO-DDS
George L. von Pragenau	MSFC/S&E-ASTR-A
Mario Rheinfurth	MSFC/S&E-AERO-DD
R. V. Sperry	Bellcomm

TABLE II: ANALYSIS OF 8-1-70 S-IVB STRUCTURAL DATA

Bellcomm, Inc.

	T + 0				T + 22			T + 52				T + 122			T + (2)098				T + (2)203				T + (2)321				T + (2)359			
RANK	N		dB	Hz	N		dB	Hz	N		dB	Hz	N			Hz	N		dB	Hz	N		dB	Hz	N		dB	Hz	N		dB	Hz
1	36	⊛	-20	17.5	38	⊛	-28	19.2	4	⊛	-34	6.8	38	⊛	-19	18.1	21	⊛	-29	10.0	23	⊛	-14	10.7	26	⊛	-1	13.1	32	⊛	-8	16.1
2	4	⊛	-35	6.8	4	⊛	-34	6.8	38	⊛	-35	19.3	22	⊛	-28	9.9	20	⊛	-31	9.9	22	⊛	-25	10.4	5	⊛	-37	7.1	30	⊛	-10	15.8
3	20	⊛	-35	9.5	20	⊛	-35	9.5	20	⊛	-37	9.6	37	⊛	-30	18.0	4	⊛	-32	6.9	4	⊛	-33	7.0	6	⊛	-40	7.2	27	⊛	-20	15.2
4	14	*	-40	8.3	44	⊛	-37	21.8	14	⊛	-39	8.4	19	⊛	-30	9.6	23	⊛	-36	10.3	11	⊛	-37	8.1	13	⊛	-40	8.2	29	⊛	-22	15.6
5	41	⊛	-44	20.3	14	⊛	-39	8.3	22	⊛	-40	9.8	4	⊛	-32	6.9	19	⊛	-36	9.7	21	⊛	-44	10.1	15	⊛	-41	8.6	28	⊛	-27	15.4
6	19	⊛	-48	9.2	19	*	-46	9.4	19	⊛	-42	9.5	14	⊛	-39	8.4	11	⊛	-39	8.0	14	⊛	-45	8.5	12	⊛	-41	8.2	43	⊛	-30	22.5
7	22	⊛	-51	9.8	21	*	-46	9.6	21	⊛	-42	9.7	11	⊛	-45	7.9	42	⊛	-40	22.1	15	⊛	-46	8.6	43	⊛	-44	22.5	38	⊛	-34	21.1
8	21		-53	9.6	22	*	-46	9.8	17	⊛	-50	9.0	17	⊛	-45	9.1	14	*	-42	8.5	5	*	-47	7.1	38	⊛	-45	21.0	31	*	-36	16.0
9	17	*	-53	8.9	45	⊛	-46	21.9	11	⊛	-50	7.9	8	⊛	-46	7.6	45	⊛	-44	22.6	6	*	-48	7.2	4	⊛	-46	7.1	13	⊛	-37	8.3
10	11	*	-54	7.9	47	⊛	-47	22.5	8	*	-52	7.5	12	*	-59	8.0	22	*	-45	10.0	8	*	-48	7.7	8	*	-50	7.7	6	*	-38	7.2
11	42	⊛	-55	21.1	17		-52	8.9	7	*	-59	7.4	6	*	-59	7.2	18	*	-46	9.3	12	*	-49	8.1	22	*	-51	10.7	5	*	-38	7.1
12	7	*	-57	7.4	11		-52	7.9	12	*	-63	8.0	16	*	-64	8.9	8	*	-47	7.7	19		-50	9.7	40	*	-52	21.6	40	⊛	-39	21.6
13	47	⊛	-57	22.5	8		-56	7.5	6	*	-63	7.2	5	*	-65	7.1	43	⊛	-52	22.3	13		-52	8.2	28	*	-52	15.3	15	*	-42	8.6
14	8		-59	7.5	7		-57	7.4	13	*	-68	8.2	20	*	-66	9.7	6		-55	7.2	18		-52	9.4	14	*	-52	8.5	42	*	-46	22.3
15	44	⊛	-64	21.5	43	⊛	-57	21.4	3	*	-70	6.5	13	*	-66	8.2	38	*	-57	21.0	20		-56	10.1	42	*	-54	22.3	44	*	-47	22.6
16	6		-66	7.2	41	⊛	-60	21.0	16		-70	8.9	7		-67	7.5	12		-58	8.1	38	*	-57	21.0	31		-56	15.9	12		-47	8.2
17	13		-67	8.2	46	*	-62	22.3	5		-70	7.1	3		-70	6.5	5		-59	7.1	43	⊛	-58	22.4	21		-59	10.2	8		-51	7.7
18	12		-67	8.0	48	*	-65	22.6	10		-71	7.8	10		-71	7.8	15		-59	8.6	42	*	-63	22.3	11		-59	8.1	4		-52	7.1
19	9		-68	7.6	6		-65	7.2	9		-75	7.6	21		-74	9.7	13		-61	8.2	9		-64	7.8	18		-60	9.4	34		-53	17.4
20	3		-69	6.5	12		-65	8.0	1		-87	4.1	30		-79	15.3	41	*	-63	21.9	49	⊛	-65	24.8	30		-60	15.5	14		-53	8.5
21	46	*	-70	22.3	13		-68	8.2	46		-91	22.4	31		-79	15.5	9		-65	7.7	40		-66	21.5	19		-61	9.8	35		-54	17.7
22	10		-71	7.8	3		-69	6.5	30		-91	15.3	9		-83	7.7	40		-66	21.4	16		-67	9.0	29		-64	15.4	39		-56	21.1
23	43	*	-71	21.1	9		-69	7.6	31		-92	15.5	39	*	-85	21.0	16		-66	9.0	10		-72	7.8	25		-67	12.0	22		-57	10.8
24	5		-73	7.0	10		-71	7.8	28		-95	12.8	1		-85	4.1	44		-71	22.6	3		-72	6.5	9		-68	7.8	41		-58	21.9
25	45		-77	21.9	5		-72	7.1	18		-97	9.2	36		-86	17.9	3		-71	6.5	30		-75	15.3	41		-69	21.9	49		-60	25.0

*Contained in 15 mode scan

⊛Contained in 9 mode stability analysis

TABLE III S-IVB OPEN-LOOP ZERO PHASE GAINS

Bellcomm, Inc.

				FREQ HZ	ZPG DB	FREQ HZ	ZPG DB	FREQ HZ	ZPG DB	FREQ HZ	ZPG DB	FREQ HZ	ZPG DB
FIRST BURN	T + 0	9 MODES	W/O PT	6.92	−47.1	--	--	9.56	−40.6	17.51	−20.7		
			WITH PT	6.92	−47.1	--	--	9.56	−40.4	17.51	−20.7		
		49 MODES		--	--	8.40	−48.5	9.57	−39.6	17.51	−20.5		
	T + 22	9 MODES	W/O PT	6.94	−46.8	8.42	−47.2	9.59	−40.8	19.12	−26.6	--	--
			WITH PT	6.91	−46.6	8.42	−46.9	9.59	−40.6	19.12	−27.7	21.33	−35.7
		49 MODES		--	--	8.43	−48.2	9.62	−38.7	19.13	−27.9	--	--
	T + 52	9 MODES	W/O PT	6.97	−47.8	--	--	9.71	−38.7	19.21	−33.5		
			WITH PT	6.97	−47.5	8.50	−57.1	9.71	−38.6	19.20	−36.8		
		49 MODES		--	--	--	--	9.70	−38.5	19.20	−36.8		
	T + 122	9 MODES	W/O PT					9.92	−31.6	18.03	−17.3		
			WITH PT					9.92	−31.5	18.03	−17.7		
		49 MODES						9.92	−31.5	18.02	−17.7		
SECOND BURN	T + 98	9 MODES	W/O PT	7.09	−47.3			10.01	−30.4			21.78	−38.7
			WITH PT	7.09	−47.0			10.00	−30.4			--	--
		49 MODES		--	--			10.01	−30.1			--	--
	T + 203	9 MODES	W/O PT					10.75	−19.2				
			WITH PT					10.75	−19.1				
		49 MODES						10.75	−19.1				
	T + 321	9 MODES	W/O PT							13.18	− 6.9		
			WITH PT							13.18	− 6.7		
		49 MODES								13.18	− 6.7		
	T + 359	9 MODES	W/O PT									15.88	− 2.6
			WITH PT									15.88	− 2.6
		49 MODES										15.88	− 2.5

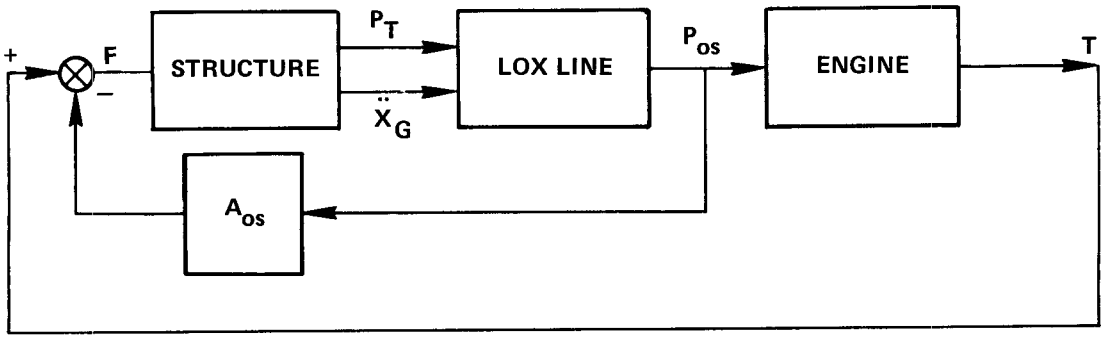

(a)

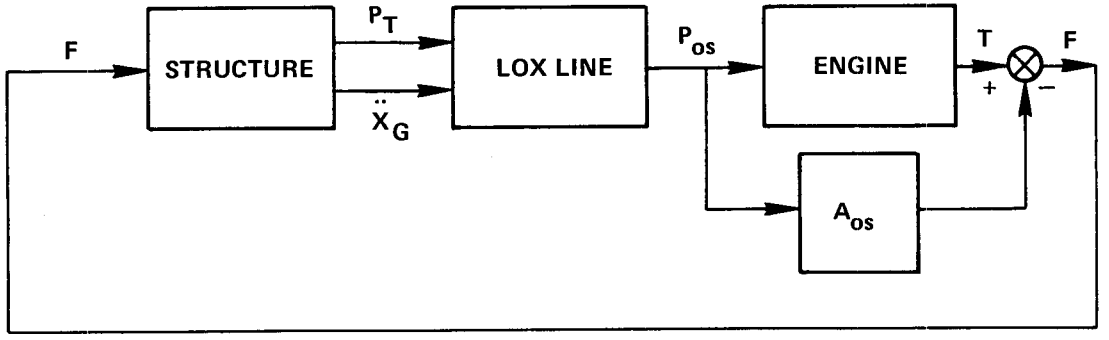

(b)

Bellcomm, Inc.

FIGURE 1 - SIMPLIFIED S-IVB POGO MODEL

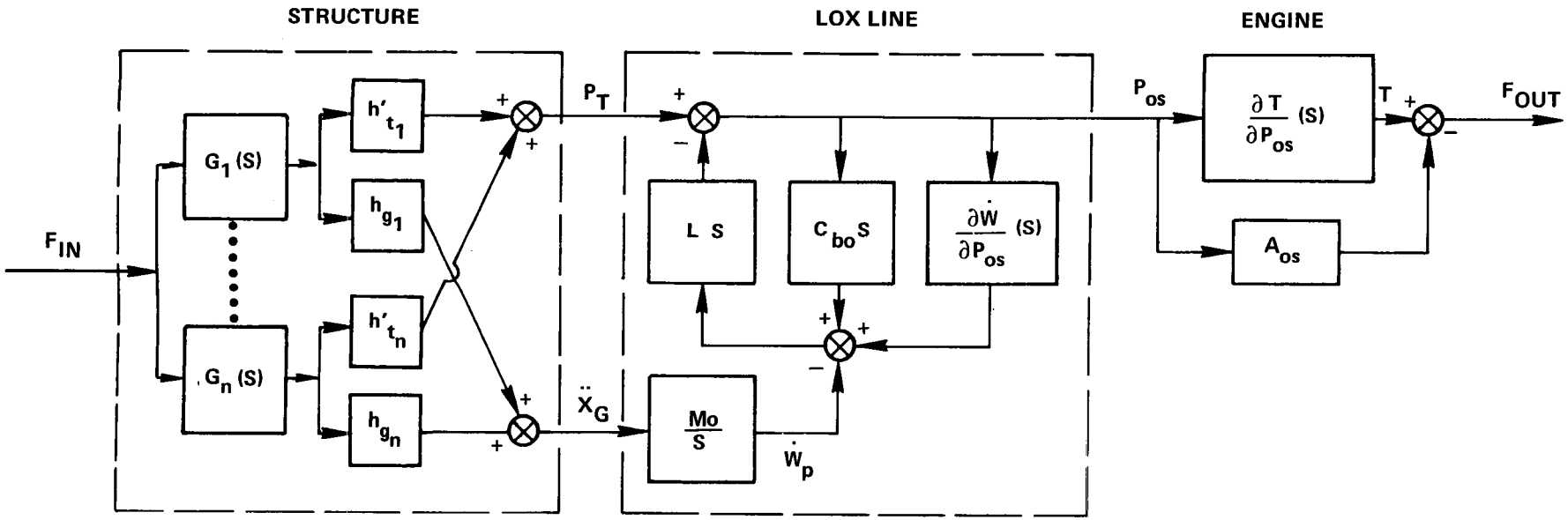

Bellcomm, Inc.

FIGURE 2 - DETAILED S-IVB POGO MODEL

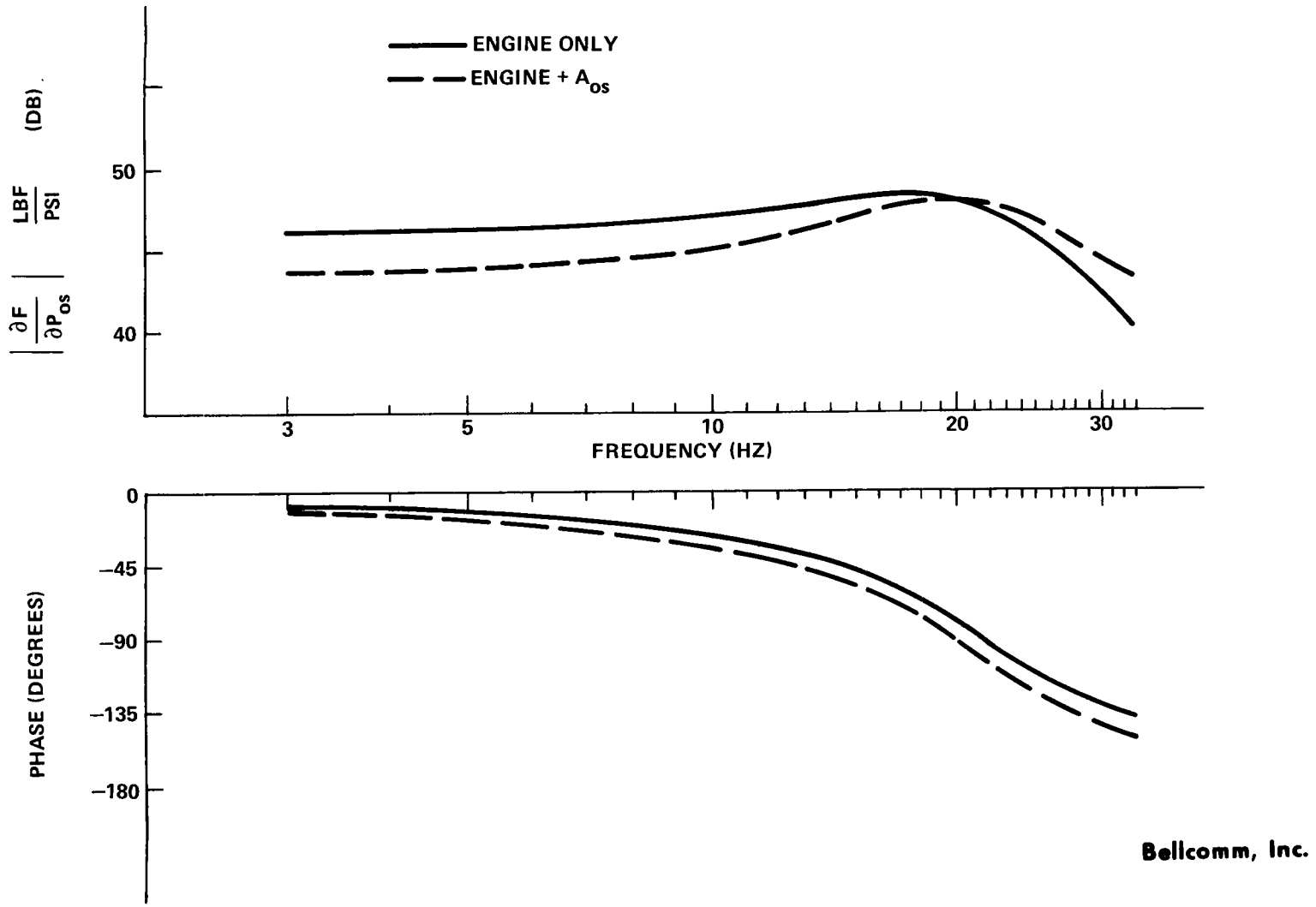

FIGURE 3 - J-2 ENGINE RESPONSE

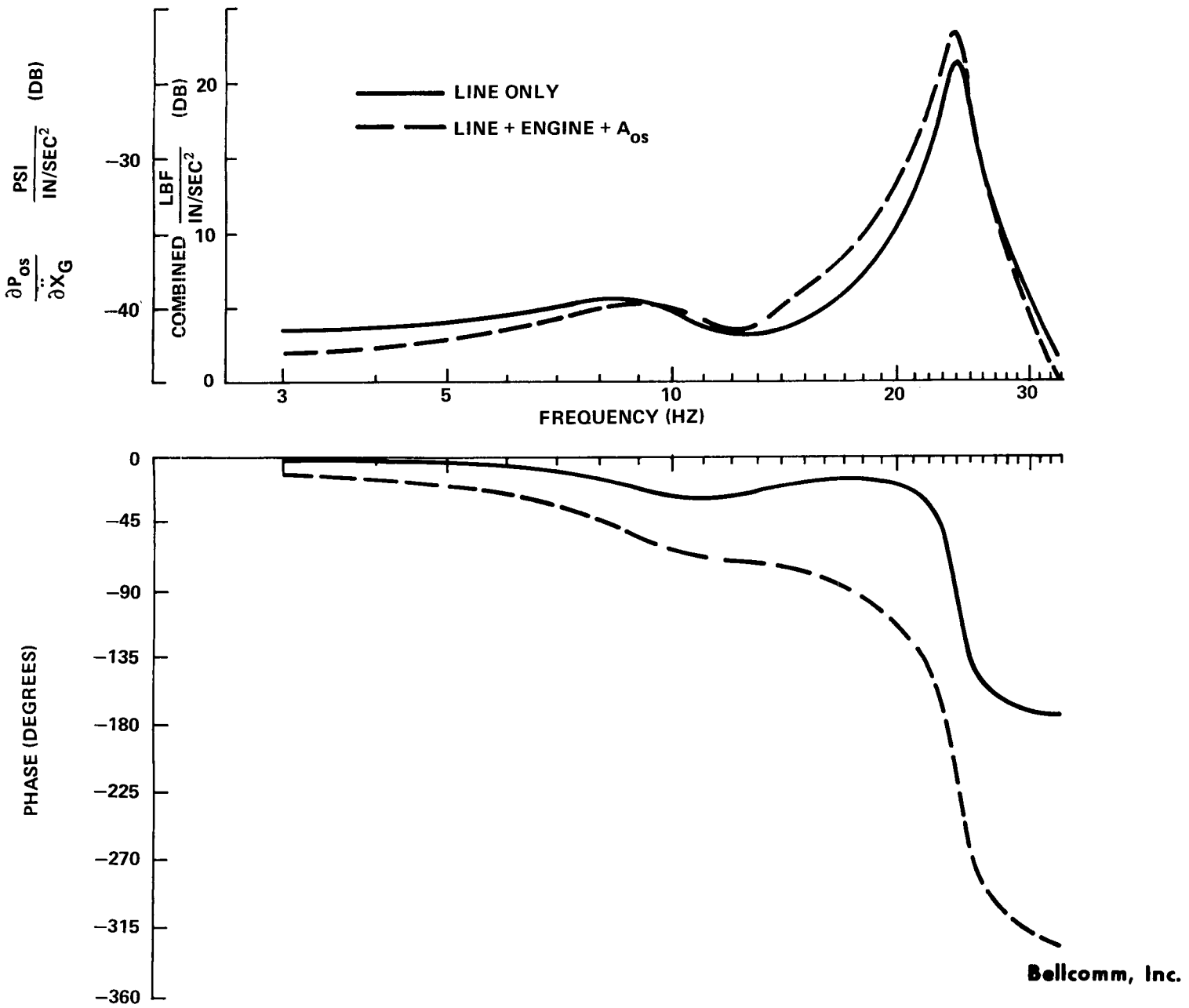

FIGURE 4 - S-IVB LOX LINE AND COMBINED RESPONSES

EXACT SOLUTION FOR CONTINUOUS LINE MODEL

$$P_{os} = \frac{1}{\cos\left(\frac{\omega\ell}{a}\right) + j\,ZK \sin\left(\frac{\omega\ell}{a}\right)} \left[P_T + j\,Z \sin\left(\frac{\omega\ell}{a}\right) \frac{\rho A \ddot{X}_G}{j\omega}\right]$$

WHERE $K = G + j\omega C_{bo}$ AND $Z = \frac{a}{Ag}$.

FOR A LINE LENGTH ℓ SMALL COMPARED TO THE ACOUSTIC WAVE LENGTH,

THAT IS, $\ell \ll \frac{a}{\omega}$ OR $\frac{\omega\ell}{a} \ll 1$

THEN $P_{os} \approx \frac{1}{1 + j\omega LK} \left[P_T + \frac{\rho\ell}{g} \ddot{X}_G\right]$.

Bellcomm, Inc.

FIGURE 5 - LOX LINE EQUATIONS

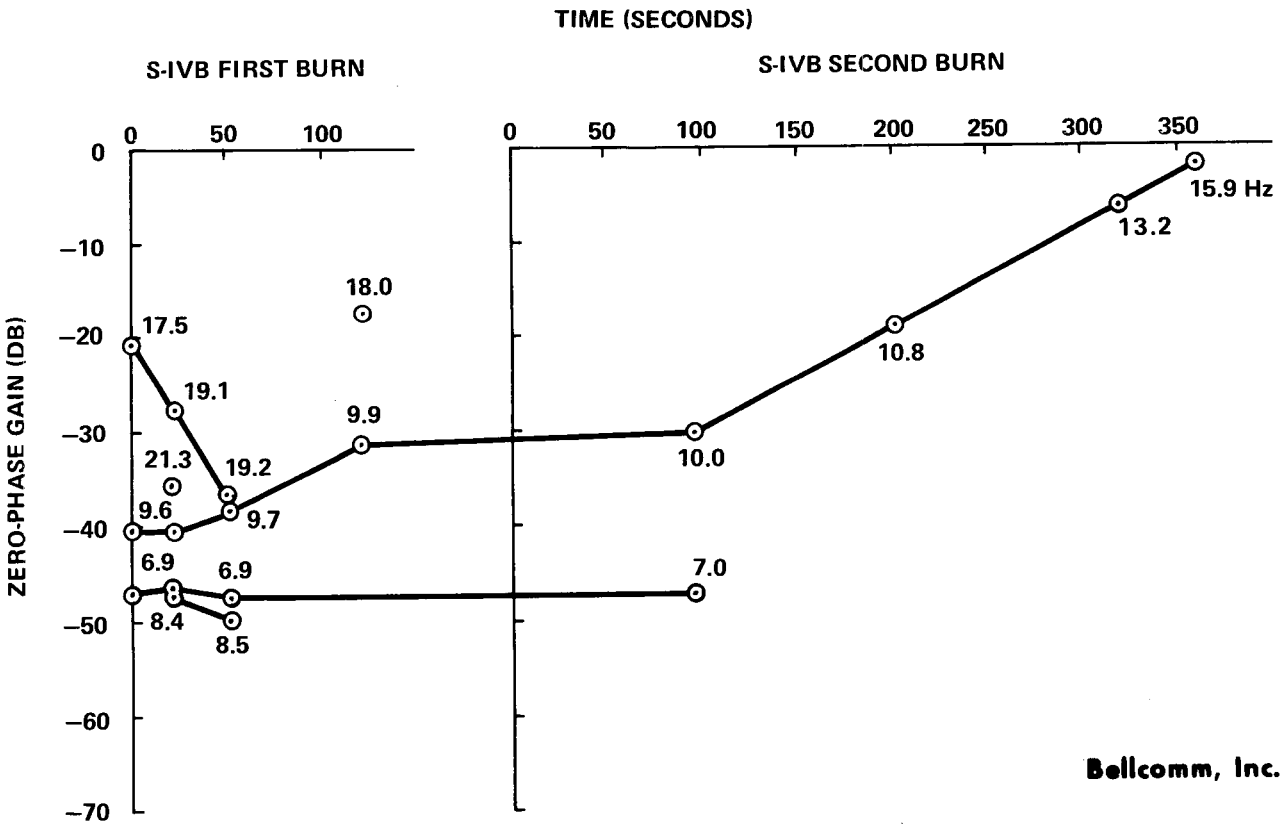

FIGURE 6 - S-IVB STABILITY MARGINS

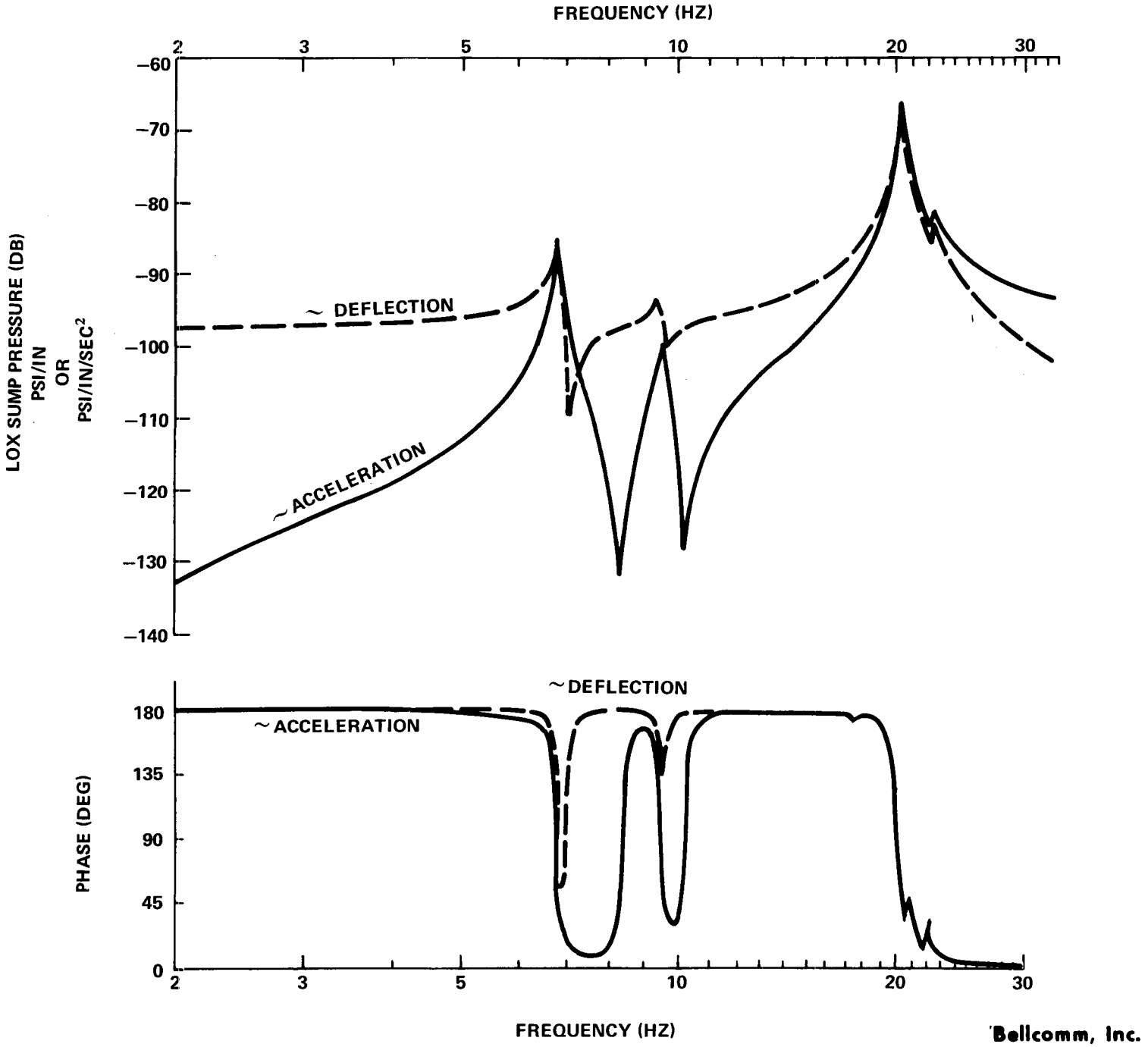

FIGURE 7 - S-IVB LOX TANK PRESSURE AT T+O